Chemical Engineering Communications

ISSN: 0098-6445 (Print) 1563-5201 (Online) Journal homepage: https://www.tandfonline.com/loi/gcec20

Kinetic study of uranium removal from aqueous solutions by macaúba biochar

Sabine Neusatz Guilhen, Suzimara Rovani, Luizildo Pitol Filho & Denise Alves Fungaro

To cite this article: Sabine Neusatz Guilhen, Suzimara Rovani, Luizildo Pitol Filho & Denise Alves Fungaro (2019) Kinetic study of uranium removal from aqueous solutions by macaúba biochar, Chemical Engineering Communications, 206:11, 1365-1377, DOI: 10.1080/00986445.2018.1533467

To link to this article: https://doi.org/10.1080/00986445.2018.1533467

CHEMICAL ENGINEERING COMMUNICATIONS
2019, VOL. 206, NO. 11, 1365–1377
https://doi.org/10.1080/00986445.2018.1533467

Taylor & Francis
Taylor & Francis Group

Kinetic study of uranium removal from aqueous solutions by macaúba biochar

Sabine Neusatz Guilhen[a], Suzimara Rovani[a], Luizildo Pitol Filho[b], and Denise Alves Fungaro[a]

[a]Instituto de Pesquisas Energéticas e Nucleares (IPEN - CNEN/SP), Cidade Universitária – CEP, São Paulo, SP, Brazil; [b]Universidade do Vale do Itajaí (UNIVALI), Itajaí, SC, Brazil

ABSTRACT

Macaúba (*Acronomia aculeata*) is a palm tree native of the Brazilian savanna and a valuable renewable source of vegetable oil for human consumption and biodiesel production. In this study, the potentiality of the macaúba endocarp for biochar (BC) production was demonstrated. Moisture, density, elemental and molecular composition, along with TGA, FTIR, and XRD analyses were performed for the endocarp. Adsorption of uranyl ions, U(VI), from aqueous solutions was studied by batch technique using BC produced by slow pyrolysis of the endocarp at 350 °C (BC350). The effect of contact time on the removal of U(VI) by BC350 was evaluated. Linear and non-linear kinetics models were employed and the best fit for the experimental data was achieved for pseudo-first order non-linear model. The adsorption equilibrium was attained after 180 min of contact time and the equilibrium adsorption capacity achieved was of 400 mg g^{-1}. Finally, BC350 was characterized by SEM, FTIR, WDXRF, and XRD techniques.

KEYWORDS

Adsorption; Biochar; Macaúba; Uranium

Introduction

Various activities in the nuclear area (mining, research, fuel cycle, nuclear medicine) generate aqueous wastes containing radioactive uranium. Recently, many uranium mining and production plants have been taken out of operation. Therefore, proper decommissioning and environmental rehabilitation are required according to the international radiation protection guidelines and standards and to national regulations (NEA/IAEA, 1999).

Treatment of contaminated wastewater and aqueous radioactive wastes is essential for environmental management and the restoration of the affected ecosystem's natural conditions. To do so, several techniques and operations have been used over the years, such as precipitation, reverse osmosis, solvent extraction, ultrafiltration, and adsorption (Sakr et al., 2003; Özdemir & Usanmaz, 2009). Among these techniques, adsorption stands out for its efficiency and specificity, allowing a simple application with low investment (IAEA, 2003).

Agriculture by-products are being studied as a sustainable solution for wastewater treatment (De Gisi et al., 2016), providing a wide range of renewable sources for the production of biochar (BC), a porous, carbon-rich material. Many studies have shown that BC can be applied for wastewater treatment because it effectively removes heavy metals from aqueous solutions (Inyang et al., 2016; Patra et al., 2016).

Biochars can be produced using the pyrolysis technique, in which the biomass is carbonized at temperatures below 700 °C in the absence of oxygen (Lehmann & Joseph, 2009). The parameters that have a direct impact on the yield and properties of the BC are the heating rate, residence time and final pyrolysis temperature (Bridgwater, 2000; Lu et al., 2009), from which the maximum temperature at which the biomass is submitted to the pyrolysis furnace, called the highest treatment temperature (HTT), has the greatest influence (Antal & Grønli, 2003; Lua et al., 2004; Özçimen & Ersoy-Meriçboyu, 2008).

CONTACT Sabine Neusatz Guilhen snguilhen@ipen.br Instituto de Pesquisas Energéticas e Nucleares (IPEN - CNEN/SP), Cidade Universitária – CEP, Av. Prof. Lineu Prestes, 2242, São Paulo, SP 05508-000, Brazil.

Supplemental data for this article can be accessed on the publisher's website.

Macaúba (*Acronomia aculeata*) is a palm tree native to the Brazilian savanna and a valuable renewable source of vegetable oil for human consumption and biodiesel production (Ratter et al., 2003). After extraction of the nut oil from the coconuts, the shell, technically referred to as the endocarp, remains as a residue. This residue can be used as a raw material for the production of BC applied for the removal of uranium from aqueous solutions (Guilhen et al., 2017a).

The process of adsorption is influenced by some factors such as pH, initial concentration, adsorbent dose and contact time. Contact time represents the physical time allowed for the contact of the phases. The time to reach adsorption equilibrium corresponds to the sufficient contact time to allow diffusion process and attachment of the adsorbate molecules onto the adsorbent.

In this study, the physical properties, elemental analysis, and molecular composition of the macaúba endocarp were evaluated. The endocarp was also characterized by thermogravimetric analysis (TGA). The BC was produced by pyrolysis of the endocarp at 350 °C under argon inert atmosphere (BC350). Fourier transform infrared spectrometer (FTIR), and X-ray diffraction (XRD) analysis were performed for both the endocarp and the BC samples, in order, to evaluate the loss of the lignocellulosic structure after pyrolysis. The morphology and inorganic composition of the BC were also analyzed. The effect of contact time on the removal efficiency of BC350 of uranyl ions, U(VI), from aqueous solutions was evaluated using the batch technique. Linear and non-linear kinetic models were used to predict the best adsorption kinetics.

Experimental

Materials

Pyrolysis of the macaúba endocarp was carried out at the Waste and Metallurgy Recycling Laboratory (LAREX, Poli/USP-SP). The endocarp was supplied by Acrotech (Viçosa, Minas Gerais).

Knife mills from Rone (FA300) and Marconi (MA340) were used for grinding the endocarp and BC, respectively. A horizontal tubular furnace from Lindberg (Blue M) with central temperature control was used for the pyrolysis of the endocarp. For the determination of uranium in the adsorbate solutions, an inductively coupled plasma optical emission spectrometer (ICP OES) from Spectro (Spectro ARCOS) was used.

Preparation of solutions and standards

All solutions were prepared using ultrapure water (18.2 MΩ cm resistivity, TOC $\leq$10.0 µg L^{-1}) and analytical grade reagents unless otherwise stated. Uranium calibration standards were prepared by dilution of a stock New Brunswick Laboratory's certified reference material solution (CRM 129-A) containing 1000 mg L^{-1} U(VI) dissolved in 1% HNO_3 (Merck).

Endocarp sample preparation

The endocarp was previously ground in a knife mill using an ASTM 3/8-inch stainless steel sieve allowing homogenization of the sample and thereby greater uniformity in carbonization. The milled material was oven-dried at 100 °C for 3 h and stored in a desiccator.

Pyrolysis of endocarp

An approximate fraction of 30 g of endocarp was processed each time in an oblong boat-like alumina crucible (13 × 4 cm) under a continuous argon flow of 40 mL min^{-1}. Before starting the heating, a 20 min purge with argon was performed. Heating was initiated with a heating rate of 5 °C min^{-1} until reaching the HTT of 350 °C, at which it remained for a residence time of 1 h.

At the end of the pyrolysis, the furnace was switched off and the sample was slowly cooled to approximately 100 °C under an inert atmosphere, then removed from the furnace to prevent condensation of vapors and stored in a desiccator until room temperature was reached. Further grinding was carried out in a knife mill using Mesh 10 mesh sieve. The ground material was packed in polypropylene tubes and identified as "BC350."

Endocarp and *BC* characterization

The moisture of the endocarp was determined using a gravimetric technique, according to the ASTM D1762-84 standard (ASTM, 2007) and the density of endocarp was determined by pycnometry using a Micromeritics Pycnometer GeoPyc 1360 (MicroMetrics, Ottawa, Canada).

Elemental analysis of the macaúba endocarp was performed on LECO elemental analyzers, TCHEN600, and CS-400 (LECO Corporation, Saint Joseph, USA). TCHEN600 is an H, O and N detector and the CS-400 is a C and S detector.

Molecular composition (cellulose, hemicellulose and lignin content) of the macaúba endocarp was determined by acid detergent fiber (ADF) and neutral detergent fiber (NDF) analysis, according to the procedure described by (Silva & Queiroz, 2002).

Thermogravimetric analysis (TGA) was used to evaluate the behavior of the pyrolytic decomposition of cellulose, hemicellulose, and lignin of the endocarp. A 10 °C min^{-1} heating rate was employed and the thermal decomposition was conducted under a N_2 atmosphere with a flow of 50 mL min^{-1}, using an alumina-port sample heated to 1000 °C. A TA Simultaneous Thermal Analyzer, model STD Q600 (TA Instruments, New Castle, USA) was used.

Fourier transform infrared spectrometer (FTIR) of macaúba endocarp and BC were performed using a Spectrum One FTIR Spectrometer PerkinElmer (PerkinElmer Inc., Waltham, USA) operating in universal attenuated total reflectance sensor (UATR). The spectra were obtained in the range 500–4000 cm^{-1}.

X-ray diffraction analysis (XRD) of endocarp and BC were recorded at room temperature using Cu-Kα radiation (λ = 1.5418 Å), 2θ between 10° and 80° and scan speed of 1° min^{-1} using a diffractometer Rigaku Multiflex (Rigaku Co, Tokyo, Japan).

Scanning electron microscopy (SEM) images of BC (coated with platinum) were recorded on a microscopy FEI Quanta 650 FEG (FEI Company, Hillsboro, Oregon, USA), at a typical acceleration voltage of 15.00 kV. Equipped with an EDS spectrometer for chemical analysis and also directional BSE detector for next-level imaging, enabling Electron Backscatter Diffraction analyses (EBSD) (Reimer & Volbert, 1979).

Semi-quantitative analysis of the BC sample was performed by wavelength dispersive X-ray fluorescence spectrometry (WDXRF), using a Zetium PANanalytical WDXRF spectrometer (Malvern PANanalytical Ltd., Royston, UK).

Sorption experiments of U(VI)

Kinetic study

Batch sorption experiments of U(VI) on macaúba BC (BC350) were undertaken in triplicates. The effect of contact time on uranium adsorption by BC350 was evaluated by varying the stirring time of the solution in contact with the adsorbent. To that end, 11 independent solutions with an initial concentration of 5.0 mg L^{-1} of U were prepared at pH 3 and brought into contact with a dose of 10.0 g L^{-1} of the adsorbent, BC350, being subjected to shaking at 130 rpm and withdrawn at predetermined time intervals to a total of 300 min. The initial concentration, pH and dose have been examined and optimized in a previous study (Guilhen et al., 2017b). The concentration of U(VI) was determined by ICP OES. Before the quantitative determination of samples after adsorption, they were previously filtered using a SCP Science 0.22 µm filter (SCP Science, Quebec, Canada). The amount of U(VI) removed by the BC was expressed as removal percentage and calculated according to equation 1.

$$\%\ Removal = \frac{(C_i - C_f)}{C_f} \times 100 \qquad (1)$$

"C_i" and "C_f" are the initial and final concentration of U(VI), respectively. The amount of U(VI) adsorption as a function of time "q_t" (mg g^{-1}) was calculated by the equation 2.

$$q_t = \frac{(C_i - C_f)}{m} \times V \qquad (2)$$

"V" is the volume of U(VI) solution and "m" is the mass of BC in grams (Kratochvil & Volesky, 1998; Tran et al., 2017).

Linear and non-linear kinetic models

Kinetic adsorption models were used to mathematically describe the adsorption process. Linear

kinetic adsorption models such as pseudo-first order (PFO) (Lagergren, 1898), pseudo-second order (PSO) (Blanchard et al., 1984; Ho & McKay, 1999), intraparticle diffusion (IPD) (Weber & Morris, 1963) and Elovich (Elovich & Zahbrova, 1939; Tran et al., 2017) were evaluated. Non-linear kinetic models of PFO (Lagergren, 1898; Ho & McKay, 1998) and PSO (Blanchard et al., 1984; Lima et al., 2015) were also evaluated. Both linear and non-linear kinetics expressions for each adsorption model are shown in Table 1.

According to linear and non-linear kinetics equations of the Table 1, "t" is the contact time (min), "q_t" is the amount of adsorbate adsorbed at time (mg g^{-1}), "q_e" is the equilibrium adsorption capacity (mg g^{-1}), "k_1" is the PFO rate constant (min^{-1}), "k_2" is the PSO rate constant (g mg^{-1} min^{-1}), "k_{int}" is the IPD rate constant (mg/(g $min^{1/2}$)), "C" is a constant associated with the thickness of the boundary layer (mg g^{-1}), "α" (mg g^{-1} min) is a initial rate constant, "β" (mg g^{-1}) is the desorption constant during any one experiment (Tran et al., 2017).

Results and discussion

Feedstock characterization

The macaúba endocarp was characterized according to the following parameters: moisture, density, elemental analysis, and molecular composition. Additionally, TGA, FTIR/UATR, and XRD analyses of the macaúba endocarp were performed.

Basic properties

Table 2 presents the main characteristics of the macaúba endocarp used as feedstock for BC production. The main constituents of plant biomass are cellulose, hemicellulose, and lignin. Biomasses with higher lignin content present a higher BC yield (Oliveira et al., 1982; Sohi et al., 2010; Zhang et al., 2010; Lee et al., 2013). Among other biomasses, such as wood fibers (28.1%) (Gwon et al., 2010), rice husk (27.0%), bamboo (25.8%), elephant grass (23.2%), Jatropha seed husk (26.0%), and sugarcane bagasse (24.9%) (Macedo et al., 2014), macaúba endocarp shows a higher lignin content (≈35%), allowing a higher yield in the BC production.

Table 1. Linear and non-linear kinetics expressions.

Models	Linear form	Non-linear form
PFO	$\log(q_e - q_t) = \log q_e - k_1 t$	$q_t = q_e.(1-\exp^{(-k_1 t)})$
PSO	$\frac{1}{q_t} = \frac{1}{k_2 q_e^2} + \frac{t}{q_e}$	$q_t = \frac{k_2 \cdot q_e^2 \cdot t}{1 + k_2 \cdot q_e \cdot t}$
IPD	$k_{int} = \frac{q_t}{t^{\frac{1}{2}}} + C$	–
ELOVICH	$q_t = \frac{1}{\beta}(ln\alpha\beta) + \frac{1}{\beta}(lnt)$	–

IPD = intraparticle diffusion; PFO = pseudo-first order; PSO = pseudo-second order.

Table 2. Physical properties, elemental analysis and molecular composition of the macaúba endocarp.

Physical properties	Moisture (%)	9.95
	Density (g cm^{-3})	1.34
Elemental analysis	C (%)	50.6
	H (%)	6.4
	N (%)	1.0
	S (%)	0.3
	O (%)	47.4
	H/C	0.13
	O/C	0.94
Molecular composition	Cellulose (%)	37.91
	Hemicellulose (%)	17.97
	Lignin (%)	34.66

Biochar productivity is directly related to the biomass density. Compared to other biomasses (Dourado et al., 2017), such as the physic nut bark (0.124 g cm^{-3}), the castor bean shell (0.171 g cm^{-3}) and the peanut bark (0.205 g cm^{-3}), the macaúba endocarp presented a much higher density (1.336 g cm^{-3}).

Also, the quality of the BC is favored by low moisture and high carbon contents (Oliveira et al., 1982). The ideal moisture content for the pyrolysis process is less than 10%, otherwise, it may alter the process heat rate and influence yields (Boateng et al., 2010; Dai et al., 2012). The moisture content found for the macaúba BC is within this requirement.

Hydrogen–carbon (H/C) and oxygen–carbon (O/C) ratios are used to determine the degree of unsaturation and the polarity of the surface of materials, respectively (Shen et al., 2018). The H/C and O/C ratios of the macaúba endocarp were similar to those found by (Macedo et al., 2014) for rice husk and sugarcane bagasse. The carbon content found for macaúba endocarp (50.6%) was somewhat higher than that found for other biomasses (rice husk, eucalyptus, miscanthus, sugarcane bagasse, bamboo), for which the carbon content ranged between 39.1 and 50.1% (Oasmaa et al., 2010; Paula et al., 2011; Rousset et al., 2011; Huang

et al., 2012). These results demonstrated the potentiality of the macaúba endocarp as feedstock for BC production.

Thermogravimetric analysis

The thermogram of macaúba endocarp can be visualized in Figure 1 and results of the thermogravimetric decomposition of the macaúba endocarp are compiled in Table 3.

The thermograms indicate that the mass loss corresponding to the first stage consists of 6.93%, while the mass loss corresponding to the subsequent stages consists of 23.21%, 28.31%, and 30.82% (second, third, and fourth stage, respectively). The first mass loss occurs between 31 and 149 °C and corresponds to the dehydration process, reaching a maximum rate at 58 °C. The subsequent decomposition step occurs between 149 and 297 °C and is characterized by the depolymerization of cellulose and hemicellulose (volatile compounds of rapid decomposition) and partial decomposition of lignin, reaching a maximum rate at 268 °C (Abdullah et al., 2010; Nasri et al., 2014). The final pyrolysis stage is characterized mainly by the decomposition of heavy components such as lignin and other aromatic structures between 297 and 400 °C, reaching a maximum rate at 334 °C. The fourth stage, from 400 to 995 °C, corresponds to the elimination of semivolatile compounds and the degradation of fixed organic compounds. The remaining 10.73% corresponds to the residual inorganic mass (ashes). The pyrolytic decomposition of the macaúba endocarp, in fact, occurs in the transitions Θ2 and Θ3 (Mackay & Roberts, 1982).

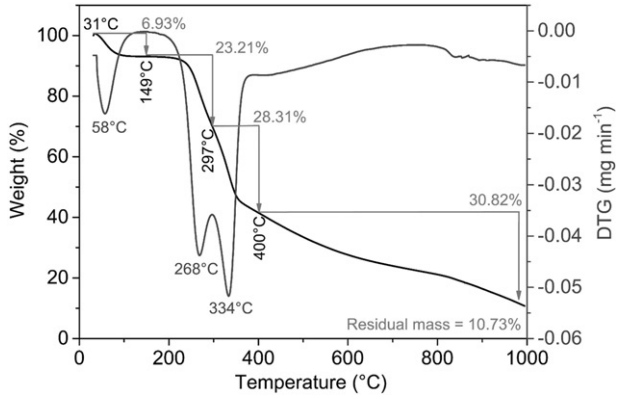

Figure 1. TG and DTG curves of the macaúba endocarp. The measures were performed under N_2 atmosphere.

Table 3. Thermal decomposition temperatures of the macaúba endocarp. The measures were performed under N_2 atmosphere.

Stages	Temperature ranges (°C)	T_{max} (°C)
Dehydration (Θ1)	31.53–149.37	58.21
Hemicellulose & Cellulose (Θ2)	149.37–297.48	268.03
Lignin (Θ3)	297.48–400.00	334.22

FTIR/UATR spectra

The macaúba endocarp is a lignocellulosic biomass that has a complex chemical structure, consisting mainly of cellulose, hemicellulose, and lignin. After pyrolysis of the endocarp at 350 °C, the lignocellulosic structure is partially decomposed. The FTIR spectra employing UATR of samples before and after pyrolysis are shown in Figure 2.

Analysing the FTIR spectra the 3600–3100 cm^{-1} region is commonly attributed to O–H stretching in hydroxyl, carboxyl, and water molecules of both the endocarp and the BC samples (Shen et al., 2018). The band in 3400 cm^{-1} for the macaúba endocarp is characteristic of hydroxyl groups (–OH) in cellulose, more specifically, the carbon 2, 3, and 6 of the glucose molecule (Barreto et al., 2010). Other bands at 2940 and 2904 cm^{-1} observed for the endocarp are associated with the C-H stretch of aliphatic groups and aromatic hydrocarbons, disappears after the pyrolytic process, suggesting the degradation of the hemicellulose structure (Chen et al., 2012; Uchimiya et al., 2013). The region between 1770 and 1650 cm^{-1} is

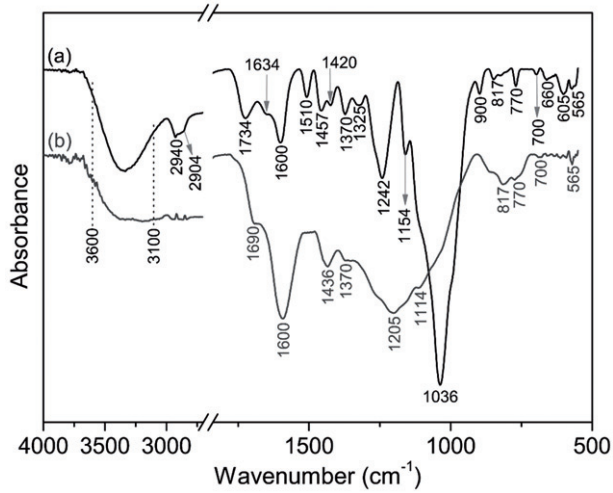

Figure 2. FTIR/UATR spectra of a) macaúba endocarp and b) biochar-BC350.

relative to the C = O stretching of carbonyl groups attributed to lignin and these bands were observed in the two spectra (Shen et al., 2018).

The bands at 1634, 1600, and 1510 cm^{-1} correspond to the C = C stretching of aromatic rings and are typical of the aromatic skeleton of lignin. The band in 1600 cm^{-1} was higher for the BC350 sample than the same band for the macaúba endocarp. This phenomenon is consistent with the pyrolytic process, which promotes the aromatization of the BC surface by the loss of polar groups (Chen et al., 2012; Uchimiya et al., 2013).

In both spectra, bands were observed in the region between 1480 and 1420 cm^{-1}. These bands can be attributed to the bending of C–H of aliphatic structures. The presence of phenolic groups in BC350 is revealed by the adsorption at the 1370 cm^{-1} band, owing to stretching O–H vibrations. O–H and C–H bending vibrations observed at 1325 cm^{-1} in the endocarp spectrum, disappear after pyrolysis in the BC350 spectrum (Chen et al., 2012; Uchimiya et al., 2013).

The bands between 1300 and 1000 cm^{-1} are related to the C–O stretch of esters with unsaturated tertiary, secondary, and primary hydroxyl groups. These bands merge in the BC350 spectrum (1205 cm^{-1}), indicating degradation of hemicellulose, cellulose, and lignin (Durán-Valle, 2012). Stretching vibration of inorganic components (Si and Al) were observed in the following bands: 1114 and 1036 cm^{-1} related to Si–O–Si asymmetric stretching and/or Si–O–C; 817 cm^{-1} associated with Si–O symmetric stretching; 770 and 700 cm^{-1} corresponds to the Si–C and Si–O–Si symmetric stretching, respectively; 565 cm^{-1} related to Si–O–Al stretching (Valadez-Gonzalez et al., 1999; Sayılkan et al., 2004; Gwon et al., 2010).

The small band at 900 cm^{-1}, in the endocarp spectrum, is characteristic of β-glycosidic linkages between the sugar units in amorphous cellulose (Corici et al., 2016). Bands between 900 and 700 cm^{-1} can be attributed to the vibration of the C–H bond in aromatic structures (Durán-Valle, 2012). The bands at 660 and 605 cm^{-1} are attributed to the out-of-plane and in-plane deformation of the ring, respectively, these bands disappear after pyrolysis indicating degradation of hemicellulose, cellulose, and lignin as seen above (Kowczyk-Sadowy et al., 2015).

Crystalline structure

The diffraction pattern corresponding to the endocarp show in Figure 3 exhibits a predominantly amorphous characteristic, with two typical peaks of an amorphous halo (2θ at 15° and 22.5°). Usually, XRD patterns characterized by an intense amorphous halo with maximum values between 20 and 23° and minimum values between 13 and 17° indicate the presence of cellulose and lignin, respectively. The BC (BC350) presents a smooth band at 2θ = 22.5°, evidencing a partial degradation of the endocarp (Vassilev et al., 2013).

SEM, EDS, EBSD, and WDXRF studies

SEM images of the BC350 sample are presented in Figure 4 and in Figure S1. The pores can be better visualized in the enlarged images (Figure 4

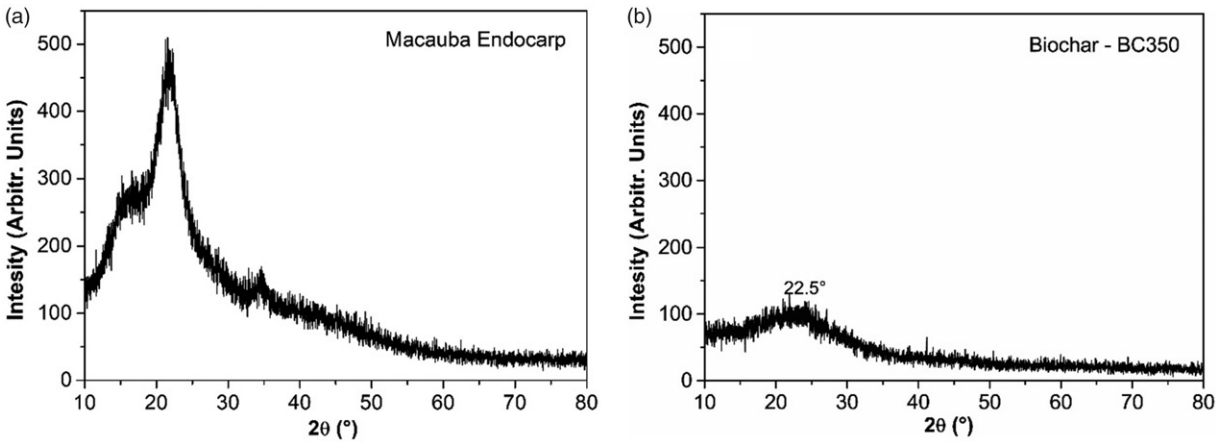

Figure 3. Diffractograms of a) macaúba endocarp and b) biochar-BC350.

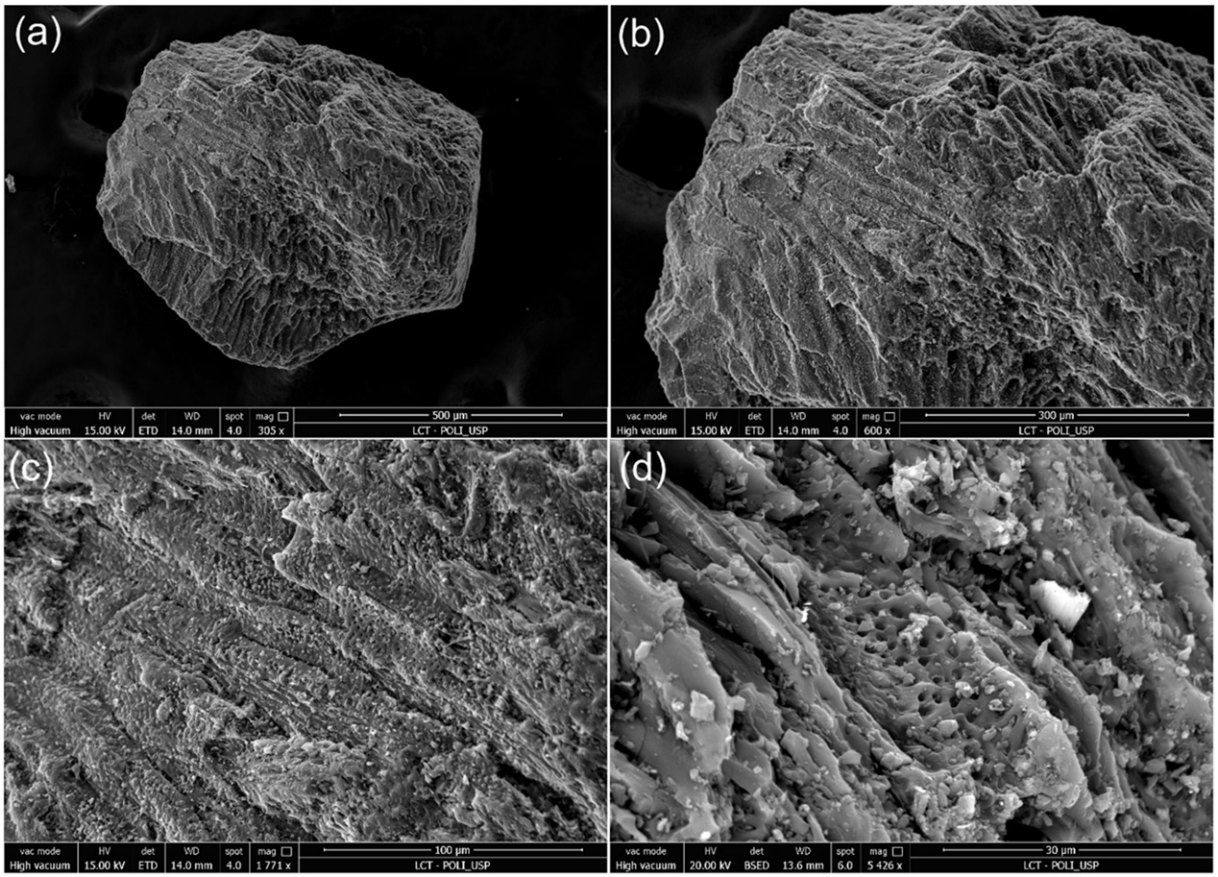

Figure 4. SEM images of biochar-BC350 with four different magnifications, a) 305x, b) 600x, c) 1771x and d) 5426x.

a–d). In spite the high heterogeneity of the BC350's surface, it is possible to observe a permeable structure given by channels formed by the transport of water vapor and volatile compounds to the surface (Bandosz, 2006).

The EBSD technique was used to detect the presence of elements or impurities on the BC350 surface. One region ("1") and 3 points ("2," "3," and "4") were selected on the surface of BC350 as shown in Figure S2. The EBSD image is generated by the emission of backscattered electrons and shows the compositional differences on the material's surface. The energy dispersive spectroscopy (EDS) technique allowed quantitative determination of the selected areas. Figure S3 represents the regions marked as "1" on the BC350 EBSD image. A predominance of carbon is observed and no significant element or impurity was detected in this region. Therefore, this region's image describes mainly the BC. Platinum was used to cover the sample and, therefore, it was also detected. Oxygen, and sodium were also observed in a lesser extent compared to carbon. Figure S4 and S5 respectively represent points "2" and "3" of Figure S2. For both, characteristic Si K-band emissions were observed, in agreement with the X-Ray fluorescence results, which are presented below.

Figure S6 represents point "4" indicated in Figure S2. Both platinum and aluminum were observed. Aluminum is present probably as an impurity, considering the operational steps for the BC350 production. Aluminum was also observed in FTIR analysis of BC. Elemental mapping by EDS allows highlighting the elements using false color. In Figure S7, it is possible to visualize the distribution of Si on the surface of BC350, corroborating with the FTIR analysis.

Table 4 presents the inorganic chemical composition of the BC350 obtained by semi-quantitative analysis using WDXRF. The results showed that the major components in the BC350 are, in order of magnitude, Si, K, and Na, making up for 78% of the inorganic chemical composition (Figure S8). S, Cl, and Ca content respond for 14% of the total ash composition, whereas the other elements (Mg, Al, P, Cr, Fe, and Zn) respond for the remaining 8% of the total

Table 4. Inorganic chemical composition of the biochar-BC350.

BC350	Content (%)
Na_2O	18.2
MgO	1.62
Al_2O_3	2.02
SiO_2	38.9
P_2O_5	1.62
SO_3	4.05
Cl	6.88
K_2O	20.6
CaO	3.24
TiO_2	ND
Cr_2O_3	0.40
MnO	ND
Fe_2O_3	1.62
NiO	<0.01
CuO	<0.01
ZnO	0.81
SrO	ND

ND = not detected.

composition. Ni and Cu couldn't be quantified and Ti, Mn, and Sr weren't detected.

According to studies reported in the literature, silica is predominantly found in the ashes of some biochars, such as those obtained from corn straw and switchgrass, while alkali metals are mostly found in biochars obtained from hardwood, which is the case of the macaúba BC (Boateng, 2007; Brewer et al., 2009).

Sorption of U(VI)

Kinetic study

Adsorption kinetics study can provide information such as the rate of adsorption, which is indicative of the adsorbent's efficiency, and the equilibrium adsorption capacity of the adsorbent. The study of adsorption kinetics is important to design industrial reactors and operation of adsorption systems (Hong et al., 2018). The adsorption velocity generally depends on the physicochemical characteristics of adsorbent and adsorbate (Rovani et al., 2018). The effect of contact time on the removal of U(VI) by BC350 is shown in Figure 5. The adsorption rate varies with the effective concentration of available sites of adsorbent. It is noted that although most of the uranyl ions had already been removed after 75 min, a minimum of 180 min of contact is required to reach the adsorption equilibrium, at which the equilibrium adsorption capacity for U(VI) was 400 mg g^{-1}, with an 80% removal efficiency. Subjecting the U(VI)/BC350 system to longer periods of contact won't entail no further improvements in adsorption.

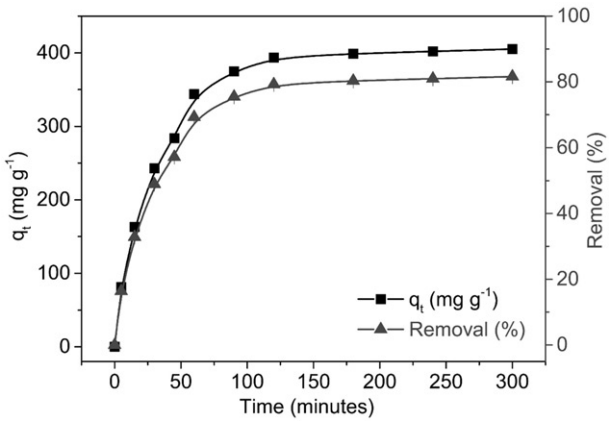

Figure 5. Effect of contact time on U(VI) adsorption by biochar-BC350.

Four linear kinetics models were used to evaluate the adsorption kinetics of U(VI) by BC350. The corresponding linear kinetic plots are shown in Figure 6.

A comparison between the calculated (linear kinetics plot) and measured (black dots) results for the U(VI)/BC350 system is shown in Figure 7.

The linear kinetic parameters of each model were derived from their respective linear kinetic plot and are presented in Table 5.

According to Table 5, the PSO model presents a better fit. This is predictable, given that the PSO equation is mathematically more linearizable. Nevertheless, although the adjusted coefficient of determination value (R^2_{adj}) for the PSO model (0.999) is closer to 1.0 compared to the R^2_{adj} value obtained for the PFO model (0.998), this difference is not statistically significant.

The values of the calculated q_e (q_e calc.) for both PFO and PSO are close to the experimentally observed value (q_e exp.). Even though the q_e calc. value for the PFO is closest to the q_e exp. value, the lack of agreement with the coefficient of determination does not allow the assignment of the best fit of the experimental data to the PFO model. Therefore, using linear models to describe the adsorption kinetics of U(VI) by BC350 is inconclusive.

The experimental data for the IPD model are arranged in two intersecting lines, indicating different stages in adsorption. In this case, both

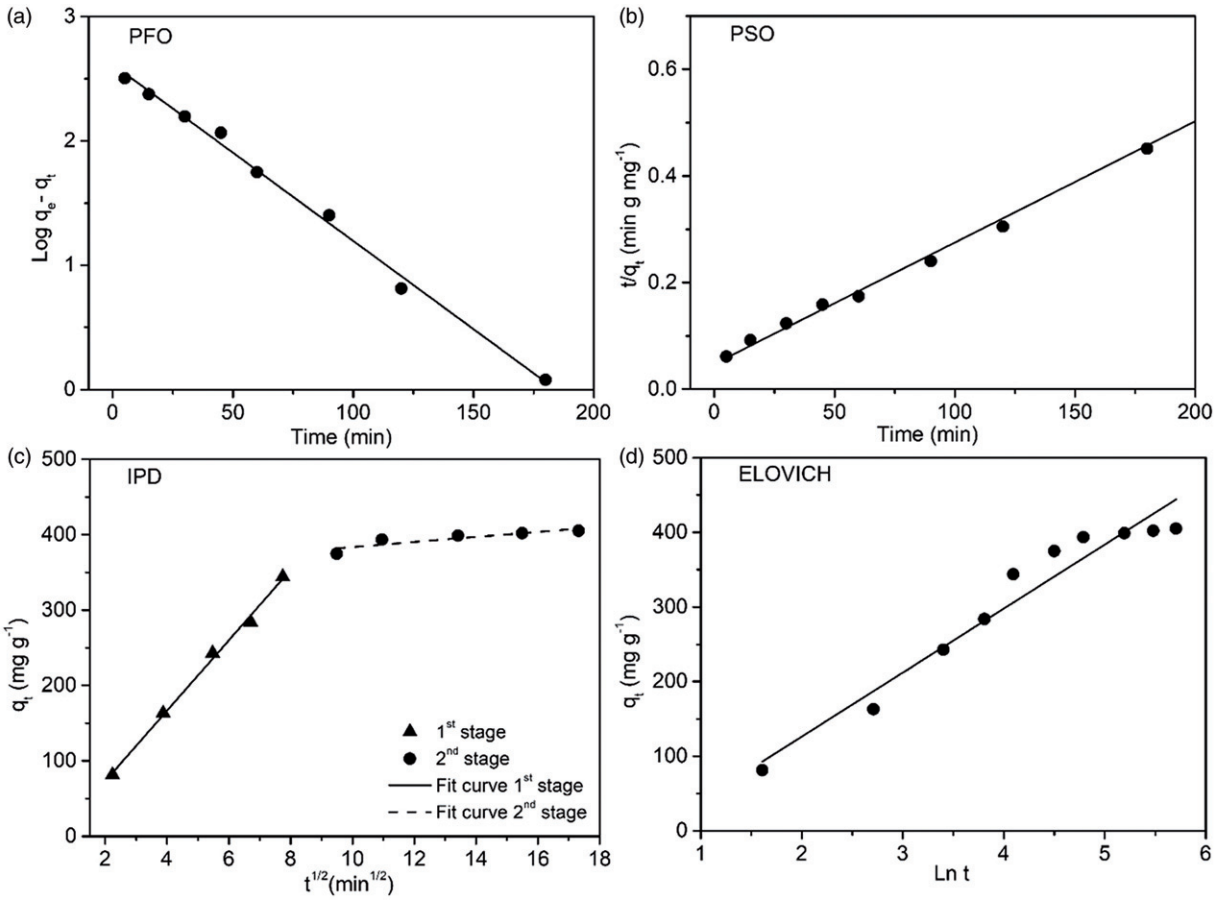

Figure 6. Linear kinetic plots, a) PFO, b) PSO, c) IPD, and d) Elovich, for adsorption of U(VI) by biochar-BC350.

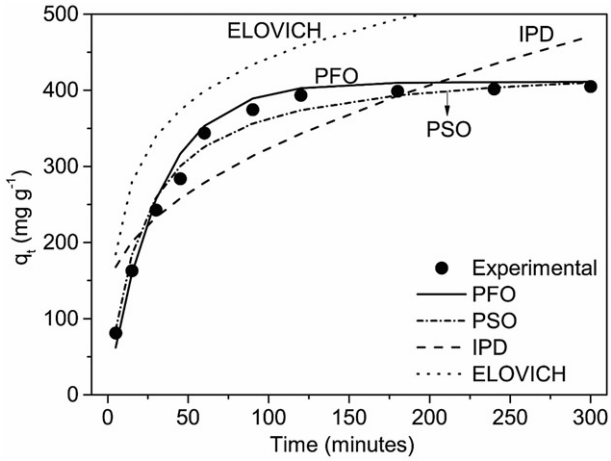

Figure 7. Linear kinetics plot for adsorption of U(VI) by biochar-BC350.

surface adsorption and IPD may contribute to the adsorption process (Zou et al., 2011). The Elovich model is usually suitable for systems in which the adsorbent presents a highly heterogeneous surface. However, the lack of adjustment of both IPD and Elovich models can be attributed to the lower values of "R^2_{adj}."

Non-linear kinetics models were also applied for experimental adjustment. Figure 8 shows the non-linear kinetic plot. The PFO and PSO non-linear regression models were employed.

The parameters of non-linear kinetic models are presented in Table 6.

The values of q_e calculated for the PFO and PSO were very different from each other and the PFO is closer to the experimentally observed value (q_e exp). In addition, the R^2_{adj} value of the PFO (0.994) shows a better adjustment of this model than the PSO one (0.991). The non-linear method allowed eliminating the discrepancies between the predictions and the experimental data of the linear method (Chowdhury & Saha, 2011). It is preferable to use the non-linear method to efficiently and effectively represent a kinetic model (Kumar, 2006).

Table 5. Linear kinetic parameters values for U(VI) onto biochar-BC350.

PFO				
k_1 (min^{-1})	–	q_e calc (mg g^{-1})	q_e exp (mg g^{-1})	R^2_{adj}
32.7 x 10^{-3}	–	411	400	0.998
PSO				
k_2 (g mg min^{-1})	h (mg g^{-1} min^{-1})	q_e calc (mg g^{-1})	q_e exp (mg g^{-1})	R^2_{adj}
1.3 x 10^{-4}	25.4	439	400	0.999
IPD				
C (mg g^{-1})	k_p (mg/(g $min^{1/2}$))	–	R^2_{adj} 1st stage	R^2_{adj} 2nd stage
20.1	3.35	–	0.995	0.728
Elovich				
α (mg g^{-1} min^{-1})	β (g mg^{-1})	–	–	R^2_{adj}
147	11.6 x 10^{-3}	–	–	0.973

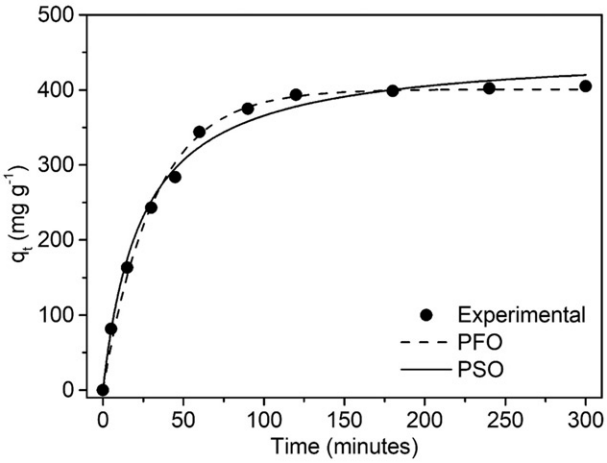

Figure 8. Non-linear kinetic plot for adsorption of U(VI) by biochar-BC350.

This way, the best fit of the experimental data can be attributed to the non-linear PFO model. This model assumes that adsorption is a chemical pseudo-reaction and the rate of the adsorption can be determined by the first-order reaction rate equation (Yang & Al-Duri, 2005). In other words, the PFO kinetics indicates that the adsorption is rate-determinant in the process (Ahmad et al., 2005).

Although the kinetics provides a greater understanding of the adsorption process, the mechanisms should be fully investigated using several different techniques (e.g. X-ray photoelectron spectroscopy "XPS" and thermogravimetric analysis/derivative thermogravimetry "TGA/DTA"), (Tran et al., 2017).

Conclusion

The macaúba endocarp exhibited promising characteristics as a potential feedstock for BC production. FTIR and XRD analysis demonstrated the degradation of the lignocellulosic structure after pyrolysis. The SEM image of the BC showed pores and high superficial heterogeneity. The predominance of carbon in the BC350 was observed in EBSD analysis. In the FTIR, EDX, EBSD, and FRX analyses were observed the Si and Al elements, while that the K and Na were observed only in the FRX analyses. The effect of contact time on the U(VI) adsorption by the BC350 was evaluated and the adsorption reached equilibrium within 180 min. According to the kinetic study, the best fit for the experimental data was achieved when the PFO non-linear model was applied. This study also signals to the potentiality of BC350 to be used as an adsorbent for U(VI) removal from aqueous solutions, since it's not only possible to achieve a high removal efficiency (80%), as the equilibrium can be reached in a shorter period (180 min instead of 24 h), allowing an optimization of the operational steps.

Acknowledgments

The authors would like to thank the Dr. Jorge Tenório from the Waste and Metallurgy Recycling Laboratory (LAREX, Poli/USP-SP), Felipe Morbi from Soleá Brasil

Table 6. Non-linear kinetic parameters values for U(VI) onto biochar-BC350.

PFO				
k_1 (min^{-1})		q_e calc (mg g^{-1})	q_e exp (mg g^{-1})	R^2_{adj}
3.15 x 10^{-2}		401	400	0.994
PSO				
k_2 (g mg^{-1} min^{-1})	h (mg g^{-1} min^{-1})	q_e calc (mg g^{-1})	q_e exp (mg g^{-1})	R^2_{adj}
9.17 x 10^{-5}	19.3	454	400	0.991

(Viçosa-MG, Brazil). This study was financed in part by the Coordenação de Aperfeiçoamento de Pessoal de Nível Superior - Brasil (CAPES) - Finance Code 001.

ORCID

Sabine Neusatz Guilhen http://orcid.org/0000-0003-2604-1225
Suzimara Rovani https://orcid.org/0000-0002-7802-1050
Luizildo Pitol Filho https://orcid.org/0000-0002-5785-0634
Denise Alves Fungaro https://orcid.org/0000-0003-1618-0264

References

Abdullah, S. S., Suzana, Y., Ahmad, M., Ramli, A., and Ismail, L. (2010). Thermogravimetry study on pyrolysis of various lignocellulosic biomass for potential hydrogen production, *Int. J. Chem. Biol. Eng.*, **3**, 750–754.

Ahmad, A. L., Sumathi, S., and Hameed, B. H. (2005). Adsorption of residue oil from palm oil mill effluent using powder and flake chitosan: Equilibrium and kinetic studies, *Water Res.*, **39**, 2483–2494.

Antal, M. J., and Grønli, M. (2003). The art, science, and technology of charcoal production, *Ind. Eng. Chem. Res.*, **42**, 1619–1640.

ASTM (2007). *Standard Test Method or Chemical Analysis of Wood Charcoal, ASTM D1762-84*. American Society for Testing and Materials International, West Conshohocken, P.A.

Bandosz, T. J. (2006). Chapter 5 desulfurization on activated carbons. In *Activated Carbon Surfaces in Environmental Remediation.*, ed Bandosz, T. J., 231–292, Elsevier, Amsterdam, The Netherlands.

Barreto, A. C. H., Esmeraldo, M. A., Rosa, D. S., Fechine, P. B. A., and Mazzetto, S. E. (2010). Cardanol biocomposites reinforced with jute fiber: Microstructure, biodegradability, and mechanical properties, *Polym. Compos.*, **31**, 1928–1937.

Blanchard, G., Maunaye, M., and Martin, G. (1984). Removal of heavy metals from waters by means of natural zeolites, *Water Res.*, **18**, 1501–1507.

Boateng, A. A. (2007). Characterization and thermal conversion of charcoal derived from Fluidized-Bed fast pyrolysis oil production of switchgrass, *Ind. Eng. Chem. Res.*, **46**, 8857–8862.

Boateng, A. A., Mullen, C. A., Goldberg, N. M., Hicks, K. B., Devine, T. E., Lima, I. M., and McMurtrey, J. E. (2010). Sustainable production of bioenergy and biochar from the straw of high-biomass soybean lines via fast pyrolysis, *Environ. Prog. Sustainable Energy*, **29**, 175–183.

Brewer, C. E., Schmidt-Rohr, K., Satrio, J. A., and Brown, R. C. (2009). Characterization of biochar from fast pyrolysis and gasification systems, *Environ. Prog. Sustainable Energy*, **28**, 386–396.

Bridgwater, A. (2000). Fast pyrolysis processes for biomass, *Renew. Sust. Energ. Rev.*, **4**, 1–73.

Chen, Y., Yang, H., Wang, X., Zhang, S., and Chen, H. (2012). Biomass-based pyrolytic polygeneration system on cotton stalk pyrolysis: Influence of temperature, *Bioresour. Technol.*, **107**, 411–418.

Chowdhury, S., and Saha, P. (2011). Adsorption kinetic modeling of safranin onto rice husk biomatrix using pseudo-first- and pseudo-second-order kinetic models: Comparison of linear and non-linear methods, *Clean Soil. Air. Water*, **39**, 274–282.

Corici, L., Ferrario, V., Pellis, A., Ebert, C., Lotteria, S., Cantone, S., Voinovich, D., and Gardossi, L. (2016). Large scale applications of immobilized enzymes call for sustainable and inexpensive solutions: Rice husks as renewable alternatives to fossil-based organic resins, *RSC Adv.*, **6**, 63256–63270.

Dai, J., Cui, H., and Grace, J. R. (2012). Biomass feeding for thermochemical reactors, *Prog. Energy Combust. Sci.*, **38**, 716–736.

Dourado, D. C., Tavares, E. L., Stroparo, E. C., Souza, K. V., Hillig, E., and Schirmer, W. N. (2017). Evaluation of the physico-chemical properties of lignocellulosic residues from biodiesel production, *Espacios*, **38**, 24.

Durán-Valle, C. J. (2012). Techniques employed in the physicochemical characterization of activated carbons. In *Characterization Techniques and Applications in the Wastewater Treatment*, ed Montoya V. H., pp. 37–55, InTech.

Elovich, S. Y., and Zahbrova, G. M. J. (1939). Mechanism of the catalytic hydrogenation of ethylene on nickel. I. Kinetics of the process, *Phys. Chem.*, **13**, 1761–1764.

De Gisi, S., Lofrano, G., Grassi, M., and Notarnicola, M. (2016). Characteristics and adsorption capacities of low-cost sorbents for wastewater treatment: A review, *SM&T*, **9**, 10–40.

Guilhen, S. N., Coleti, J., Tenório, J. A. S., and Fungaro, D. A. (2017b). Influence of pyrolytic temperature on uranium adsorption capability by biochar derived from macauba coconut residue. In *8th International Nuclear Atlantic Conference, INAC.* (Belo Horizonte, MG, Brazil), p. 1. ABEN (Associação Brasileira de Energia Nuclear) General Chair: Antonio Teixeira e Silva and Co-Chair: Hugo Cezar Rezende.

Guilhen, S. N., Ortiz, N., Fungaro, D. A., and Masek, O. (2017a). Pyrolytic temperature evaluation of macauba biochar for uranium adsorption from aqueous solutions. In *Biochar: Production, Characterization and Applications*, eds., Franco Berruti, Ondrej Masek, and Raffaella Ocone, p. 1, ECI (Engeneering Conferences International) Digital Archives: Alba, Italy.

Gwon, J. G., Lee, S. Y., Doh, G. H., and Kim, J. H. (2010). Characterization of chemically modified wood fibers using FTIR spectroscopy for biocomposites, *J. Appl. Polym. Sci.*, **116**, 3212–3219.

Ho, Y. S., and McKay, G. (1998). Sorption of dye from aqueous solution by peat, *Chem. Eng. J.*, **70**, 115–124.

Ho, Y. S., and McKay, G. (1999). Pseudo-second order model for sorption processes, *Process Biochem.*, **34**, 451–465.

Hong, Y.-S., Sin, K.-R., Ri, Y.-U., Pak, J.-S., Jon, Y., Kim, C.-S., Jang, C.-S., Ju, H.-R., and Ri, S.-H. (2018). A new KineticModelfor multicomponent adsorptionin batch systems, *ChemRxiv*. https://doi.org/10.26434/chemrxiv.5899393.v2

Huang, Y. F., Chen, W. R., Chiueh, P. T., Kuan, W. H., and Lo, S. L. (2012). Microwave torrefaction of rice straw and pennisetum, *Bioresour. Technol.*, **123**, 1–7.

IAEA. (2003). *Combined Methods for Liquid Radioactive Waste Treatment: Final Report of a Co-ordinated Research Project, 1997–2001*. (International Atomic Energy Agency, Vienna, Austria).

Inyang, M. I., Gao, B., Yao, Y., Xue, Y., Zimmerman, A., Mosa, A., Pullammanappallil, P., Ok, Y. S., and Cao, X. (2016). A review of biochar as a low-cost adsorbent for aqueous heavy metal removal, *Crit. Rev. Environ. Sci.Technol.*, **46**, 406–433.

Kowczyk-Sadowy, M., Świsłocka, R., Lewandowska, H., Piekut, J., and Lewandowski, W. (2015). Spectroscopic (FT-IR, FT-Raman, 1H- and 13C-NMR), theoretical and microbiological study of trans o-coumaric acid and alkali metal o-coumarates, *Molecules*, **20**, 3146–3169.

Kratochvil, D., and Volesky, B. (1998). Advances in the biosorption of heavy metals, *Trends Biotechnol.*, **16**, 291–300.

Kumar, K. V. (2006). Linear and non-linear regression analysis for the sorption kinetics of methylene blue onto activated carbon, *J. Hazard. Mater.*, **137**, 1538–1544.

Lagergren, S. (1898). Zur theorie der sogenannten adsorption geloster stoffe, *Kungliga Svenska Vetenskapsakademiens Handlingar*, **24**, 1–39.

Lee, Y., Park, J., Ryu, C., Gang, K. S., Yang, W., Park, Y.-K., Jung, J., and Hyun, S. (2013). Comparison of biochar properties from biomass residues produced by slow pyrolysis at 500 °C, *Bioresour. Technol.*, **148**, 196–201.

Lehmann, J., and Joseph, S. (2009). Biochar for environmental management: An introduction. In *Biochar for Environmental Management Science and Technology*, eds J. Lehmann, & S. Joseph, pp. 1–12, Earthscan Publications Ltd, London-Sterling,VA.

Lima, É. C., Adebayo, M. A., and Machado, F. M. (2015). Kinetic and equilibrium models of adsorption. In *Carbon Nanomaterials as Adsorbents for Environmental and Biological Applications*, eds C. P. Bergmann, & F. M. Machado, eds., pp. 33–69, Springer International Publishing, Cham.

Lu, Q., Li, W.-Z., and Zhu, X.-F. (2009). Overview of fuel properties of biomass fast pyrolysis oils, *Energy Convers. Manage.* **50**, 1376–1383.

Lua, A. C., Yang, T., and Guo, J. (2004). Effects of pyrolysis conditions on the properties of activated carbons prepared from pistachio-nut shells, *J. Anal. Appl. Pyrol.*, **72**, 279–287.

Macedo, L. A. D., Rousset, P. L. A., and Vale, A. T. D. (2014). Effect of biomass composition on the condensable gas yield from torrefaction of plant residues, *Pesq. Flor. Bras.*, **34**, 417–424.

Mackay, D. M., and Roberts, P. V. (1982). The dependence of char and carbon yield on lignocellulosic precursor composition, *Carbon*, **20**, 87–94.

Nasri, N. S., Zaini, M. A. A., Mohsin, R., Dadum, H. U., and Musa, A. M. (2014). Synthesis and characterization of bio-based porous carbons by two step physical activation with CO2, *J. Teknol.*, **68**, 5–9.

NEA/IAEA. (1999). *Environmental Activities in Uranium Mining and Milling*. OECD Publications Service, Paris, France.

Oasmaa, A., Solantausta, Y., Arpiainen, V., Kuoppala, E., and Sipilä, K. (2010). Fast pyrolysis bio-oils from wood and agricultural residues, *Energy Fuels*, **24**, 1380–1388.

Oliveira, J. B., Gomes, P. A., and Almeida, M. R. (1982). Estudos preliminares de normalização de testes de controle de qualidade do carvão vegetal. In *Carvão Vegetal: Destilação Propriedades e Controle de Qualidade*, pp. 7–38, CETEC, Belo Horizonte, MG, Brazil.

Özçimen, D., and Ersoy-Meriçboyu, A. (2008). A study on the carbonization of grapeseed and chestnut shell, *Fuel Process. Technol.*, **89**, 1041–1046.

Özdemir, T., and Usanmaz, A. (2009). Use of poly(methyl methacrylate) in radioactive waste management: I. Radiation stability and degradation, *Prog. Nucl. Energy*, **51**, 240–245.

Patra, J. M., Panda, S. S., and Dhal, N. K. (2016). Biochar as a low-cost adsorbent for heavy metal removal: A review, *Int. J. Res. Biosci.*, **5**, 1–7.

Paula, L. E. de R. e., Trugilho, P. F., Napoli, A., and Bianchi, M. L. (2011). Characterization of residues from plant biomass for use in energy generation, *CERNE*, **17**, 237–246.

Ratter, J. A., Bridgwater, S., and Ribeiro, J. F. (2003). Analysis of the floristic composition of the brazilian cerrado vegetation III: Comparison of the woody vegetation of 376 areas, *Edinb. J. Bot.*, **60**, 57–109.

Reimer, L., and Volbert, B. (1979). Detector system for backscattered electrons by conversion to secondary electrons, *Scanning*, **2**, 238–248.

Rousset, P., Aguiar, C., Labbé, N., and Commandré, J.-M. (2011). Enhancing the combustible properties of bamboo by torrefaction, *Bioresour. Technol.*, **102**, 8225–8231.

Rovani, S., Santos, J. J., Corio, P., and Fungaro, D. A. (2018). Highly pure silica nanoparticles with high adsorption capacity obtained from sugarcane waste ash, *ACS Omega*, **3**, 2618–2627.

Sakr, K., Sayed, M. S., and Hafez, M. B. (2003). Immobilization of radioactive waste in mixture of cement, clay and polymer, *J. Radioanal. Nucl. Chem*, **256**, 179–184.

Sayılkan, H., Erdemoğlu, S., Şener, Ş., Sayılkan, F., Akarsu, M., and Erdemoğlu, M. (2004). Surface modification of pyrophyllite with amino silane coupling agent for the removal of 4-nitrophenol from aqueous solutions, *J. Colloid Interface Sci*., **275**, 530–538.

Shen, J., Huang, G., An, C., Xin, X., Huang, C., and Rosendahl, S. (2018). Removal of tetrabromobisphenol a by adsorption on pinecone-derived activated charcoals: Synchrotron FTIR, kinetics and surface functionality analyses, *Bioresour. Technol*., **247**, 812–820.

Silva, D. J., and Queiroz, A. C. D. (2002). *Análise de Alimentos: Métodos Químicos e Biológicos*. UFV-Imprensa Universitária, Viçosa, MG, Brazil.

Sohi, S. P., Krull, E., Lopez-Capel, E., and Bol, R. (2010). A review of biochar and its use and function in soil, *Adv. Agron*., **105**, 47–82.

Tran, H. N., You, S.-J., Hosseini-Bandegharaei, A., and Chao, H.-P. (2017). Mistakes and inconsistencies regarding adsorption of contaminants from aqueous solutions: A critical review, *Water Res*., **120**, 88–116.

Uchimiya, M., Orlov, A., Ramakrishnan, G., and Sistani, K. (2013). In situ and ex situ spectroscopic monitoring of biochar's surface functional groups, *J. Anal. Appl. Pyrol*., **102**, 53–59.

Valadez-Gonzalez, A., Cervantes-Uc, J. M., Olayo, R., and Herrera-Franco, P. J. (1999). Chemical modification of henequén fibers with an organosilane coupling agent, *Compos. B Eng*., **30**, 321–331.

Vassilev, S. V., Baxter, D., Andersen, L. K., and Vassileva, C. G. (2013). An overview of the composition and application of biomass ash. Part 1. Phase–mineral and chemical composition and classification, *Fuel*, **105**, 40–76.

Weber, W. J., and Morris, J. C. (1963). Kinetics of adsorption on carbon from solution, *J. Sanit. Eng. Div*., **89**, 31–60.

Yang, X., and Al-Duri, B. (2005). Kinetic modeling of liquid-phase adsorption of reactive dyes on activated carbon, *J Colloid Interface Sci*., **287**, 25–34.

Zhang, L., Xu, C., (Charles), and Champagne, P. (2010). Overview of recent advances in thermo-chemical conversion of biomass, *Ener. Convers. Manage*., **51**, 969–982.

Zou, W., Li, K., Bai, H., Shi, X., and Han, R. (2011). Enhanced cationic dyes removal from aqueous solution by oxalic acid modified rice husk, *J. Chem. Eng. Data*, **56**, 1882–1891.